西 南 交 通 大 学 学 报

第 58 卷 第 5 期
2 0 2 3 年 10 月

JOURNAL OF SOUTHWEST JIAOTONG UNIVERSITY

Vol. 58 No. 5
Oct. 2 0 2 3

ISSN: 0258-2724 **DOI：10.35741/issn.0258-2724.58.5.4**

Research article

Engineering

TRANSIENT DYNAMIC STABILITY ANALYSIS OF HYBRID RENEWABLE ENERGY POWER GENERATION USING A RECURRENT-BASED DEEP NEURAL NETWORK WITH AN OPTIMIZATION ALGORITHM

使用基于循环的深度神经网络和优化算法对混合可再生能源发电进行瞬态动态稳定性分析

J. Vinothkumar [a,*], R. Thamizhselvan [b]

[a] Asst. Professor, Department of Electrical Engineering, Annamalai University
Annamalai Nagar, Chidambaram, Tamil Nadu 608002, India, *vinusugan@gmail.com*

[b] Associate Professor, Department of Electrical Engineering, Annamalai University
Annamalai Nagar, Chidambaram, Tamil Nadu 608002, India, *rt10535@annamalaiuniversity.ac.in*

Received: August 6, 2023 ▪ Review: August 18, 2023
▪ Accepted: September 24, 2023 ▪ Published: October 30, 2023

Abstract

Voltage source converters (VSCs) in large interconnected microgrids may use non-communication-based droop control to share the total power demand in the ratio of their droop coefficients. However, a constant droop ratio restricts the power delivery capability of the VSCs, although surplus power may be available in their respective sources. This research proposed a dynamic modeling and control strategy for a sustainable microgrid, principally powered by multiple renewable energy sources, rooftop solar panels, photovoltaic cells, floating PV, solar PV with grid, and energy storage scheme. The adaptive droop control algorithm dynamically changes the droop coefficients of the VSCs to ensure maximum utilization of the available resources in each microgrid under different operating modes. A hybrid flyback-Cuk converter is used to reduce switching losses and improve the duty cycle range over which voltage can be stepped down, which ultimately leads to an increase in efficiency. The interval-fuzzy type 3 Sugeno controller functions to regulate the output signal by obtaining the duty cycle value. Chaotic Grey Wolf Optimization Algorithm tuned Fuzzy type-3 controllers under dynamic conditions, i.e., sudden irradiation variations, deep voltage sag/swell, etc. Recurrent neural networks (RNNs) are suggested for multivariate applications, especially for systems with unclear and complex dynamics. The adaptive Lyapunov function method is proposed to mitigate transient stability issues in the presence of an RES-connected system. To minimize network loss, a heuristic-based optimization model of the renewable energy penetration capacity of the AC-DC hybrid grid is established considering transient stability constraints. The proposed work was implemented using Matlab/Simulink software. The battery voltage of the work produces constant values of 220.5V, SOC produced in this work is 99.994%, and the current and voltage produced in this work are 2000A and 1050 Vrms, respectively. Accordingly, the proposed work is validated from simulation results that the proposed control method increases the use of renewable energy sources within microgrids and reduces energy imports from the utility grid. Consequently, the results can achieve all

required functions efficiently with minimum losses over a high range of duty cycles.

Keywords: Voltage Source Converters, Photovoltaic Cells, Solar Panels, Flyback-Cuk Converter, AC-DC Hybrid Grid, Adaptive Lyapunov Function, Interval-Fuzzy Type 3 Sugeno Controller, Heuristic-Based Optimization

摘要 大型互连微电网中的电压源变流器（VSC）可以使用基于非通信的下垂控制来按照其下垂系数的比率分担总功率需求。然而，恒定的下降比限制了 VSC 的功率传输能力，尽管它们各自的源中可能有剩余功率。本研究提出了可持续微电网的动态建模和控制策略，主要由多种可再生能源、屋顶太阳能电池板、光伏电池、浮动光伏、并网太阳能光伏和储能方案供电。自适应下垂控制算法动态改变 VSC 的下垂系数，以确保不同运行模式下每个微电网的可用资源得到最大利用。混合反激式库克转换器用于减少开关损耗并改善可降低电压的占空比范围，从而最终提高效率。区间模糊 3 型管野控制器的功能是通过获取占空比值来调节输出信号。混沌灰狼优化算法在动态条件下调整模糊 3 型控制器，即突然的辐照变化、深度电压骤降/骤升等。建议将循环神经网络（循环神经网络）用于多变量应用，特别是对于动态不明确且复杂的系统。提出了自适应李亚普诺夫函数方法来缓解 RES 连接系统中的瞬态稳定性问题。为了最大限度地减少网络损耗，考虑暂态稳定性约束，建立了基于启发式的交直流混合电网可再生能源渗透能力优化模型。所提出的工作是使用 Matlab/仿真软件软件实现的。本工作的电池电压产生恒定值 220.5 V，本工作产生的 SOC 为 99.994%，本工作产生的电流和电压分别为 2000A 和 1050 有效值。因此，仿真结果验证了所提出的工作，即所提出的控制方法增加了微电网内可再生能源的使用，并减少了从公用电网的能源进口。因此，结果可以在大工作周期范围内以最小的损耗有效地实现所有所需的功能。

关键词: 电压源转换器、光伏电池、太阳能电池板、反激式库克转换器、交直流混合电网、自适应李亚普诺夫函数、区间模糊 3 型管野控制器、启发式优化

I. INTRODUCTION

The electric power system has undergone significant changes due to the rise of distributed generation installations and the shift toward renewable energy sources [1]. However, the integration of renewable energy into the system presents challenges such as stochastic production, power electronics, and instability. While solar and wind energy contribute significantly, their unpredictable nature hinders reliance on them alone [2]. Grid codes impose technical guidelines, ensuring grid stability even during faults. However, because of their nonlinear and irregular nature, renewable energy supplies can make it more difficult to provide off-grid places with electricity [3]. These difficulties include decreased reliability, control complexity, design issues, instability, and lower energy [4]. These issues are challenging nonlinear optimization issues. Optimization is the process of using hybrid RESs in the best or most cost-efficient way possible [5]. To optimize the use of hybrid renewable energy systems, nonlinear optimization becomes essential. Recently, advancements in PV systems with battery-based storage have gained attention, but they face limitations in terms of lifespan and efficiency [6]. To address these issues, research on superconducting magnetic energy storage (SMES) technology based on photovoltaic systems has been conducted. Energy management in hybrid AC/DC microgrids is complex, and efficient techniques are required to achieve optimal performance [7].

Recent technological advancements in PV systems with battery-based storage systems have received considerable attention. However, their short lifespan, constrained power size, and low efficiency are the main problems. To address these prior drawbacks, new superconducting magnetic energy storage (SMES) technology based on photovoltaic systems has been developed and researched [8]. The incorporation of RES into the microgrid operation can have several positive effects, including reduced planning expenses for transmission extension, cost savings, improved technology, and higher power quality services. However, the system's optimal energy management would be more difficult and intricate. As a result, an efficient energy management technique is presented for the best management of hybrid AC/DC

microgrids [9]. For the first time, a new machine learning-enabled heuristic approach framework has been created to not only speed up the algorithm convergence but also improve its correctness. A current-source-inverter interline dynamic voltage restorer (CSI-IDVR) based on superconducting magnetic energy storage (SMES) is suggested to effectively use renewable energy during voltage sags and decrease energy storage capacity [10]. To suppress voltage oscillations and ensure the transient stability of sensitive loads and renewable power generators during asymmetric grid breakdowns, CSI-based voltage dual control is created and implemented.

The RES system is included in [11] along with solar-thermal, conventional-thermal, wind, and electric vehicle (EV) energy sources and is given the proper system nonlinearities for a realistic approach. Parallel optimization of the secondary controller gains is accomplished using the magneto-tactic bacteria optimization (MBO) technique. The Salp swarm algorithm was used to optimize the parameters in the proportional integral derivative (PID) and fuzzy-aided PID (FPID) controllers [12]. For load frequency control, the tilt-integral-derivative with derivative filter (TIDF) controller is tuned using Harris hawks optimization technique [13]. An energy management system was created and developed using fuzzy logic controllers to maximize the use of renewable sources and minimize power loss (FLC). The FLC continuously monitors the load demand, creates control signals for switching based on fuzzy knowledge, and guarantees that the load is effectively supplied with energy [14]. A grasshopper optimization algorithm-based fuzzy PD-PI controller (FPD-PI) was developed to analyze frequency control and optimize the FPD-PI controller gains to reduce frequency variations and enable high DG penetration [15]. In this study, the stability of the microgrid operating with the proposed adaptive droop controller is determined using the change in dominant eigenvalue locations with dynamic changes in the droop ratio of the VSCs. The rest of the work is organized as follows section 2 reveals the literature survey of the study, section 3 portrays the problem definition and motivation of the research, and Section 4 illustrates the proposed research methodology. Section 5 demonstrates the experimentation and results, and section 6 reveals the conclusion of the research.

II. LITERATURE SURVEY

The literature survey provides an overview of various studies and research related to the use of hybrid energy systems for residential applications and their impact on academic performance. An upgraded multi-objective PSO algorithm was proposed in [16] to optimize hybrid energy systems, considering cost reduction and power supply reliability. [17] A two-stage multi-objective stochastic-robust hybrid optimization model was developed for a hybrid CCHP system. Constraints on the output current of IBGs were considered while examining transient behavior [18]. A Gaussian process regression-based predictive model was developed for online transient stability assessment [19]. A novel nonlinear control technique for thyristor-controlled series capacitors (TCSCs) was proposed in [20]. A current-source-inverter interline dynamic voltage restorer (CSI-IDVR) based on SMES was suggested to effectively utilize renewable energy during voltage sags [10]. Garra Rufa Fish optimization (GRFO) with the iForest approach was used in [21] for controller parameter optimization. A hybrid wind-pV farm was used as STATCOM to control oscillations in a two-area power system [22]. An evaluation technique was proposed in [23] to assess renewable energy penetration capacity. An energy management plan was presented for hybrid devices [24].

These studies collectively contribute to understanding the significance of hybrid energy systems in residential applications and their impact on academic performance and system stability, emphasizing the importance of optimizing such systems for efficiency, reliability, and sustainability in the 21st century.

III. RESEARCH PROBLEM DEFINITION AND MOTIVATION

Energy is a vital factor for the progress and development of modern societies, but heavy reliance on fossil fuels raises concerns about their future availability and the environmental impact of greenhouse gas emissions. Isolated rural areas often depend on diesel generators for energy supply, but rising fuel costs and transportation expenses make this option economically challenging. As a result, there is a growing interest in alternative fuels and renewable energy sources to address energy shortages and environmental issues. Developing hybrid renewable energy systems, both off-grid and grid-connected, has emerged as a promising solution for developing countries facing economic and energy crises. However, the development of such systems comes with technical and economic challenges that require proper control techniques, particularly in

standalone and grid-connected modes. Energy management techniques are also necessary to ensure efficient operation and system performance because load demand variations can introduce frequency and power fluctuations. With the increasing integration of renewable energy sources, ensuring transient stability becomes crucial to avoid major outages and economic losses. This research focuses on analyzing transient stability and proposes improved control methods for different power generations to enhance renewable energy penetration capacity in power grids.

IV. Proposed Research Methodology

The microgrid is a key technology for integrating distributed energy resources, energy storage systems, and loads. While renewable energy is becoming more essential for utility companies, end users, and governments, the issues associated with renewable energy use must be addressed, given the unpredictability, intermittency, and low energy density of a single renewable energy source. Microgrids based on renewable resources have been intensively researched to reduce global warming and greenhouse gas emissions. A direct current microgrid includes photovoltaic control systems, wind- and battery-based renewable energy systems, and supercapacitor-based energy storage systems. The dynamic performance of the power system depends on its ability to maintain the desired level of stability and security under various disturbances (e.g., short circuits, sudden loss of large generation units, etc.). This paper focuses on transient (or large signal rotor angle) stability, which can be considered one of the most important types of power stability phenomena. The novelty in this study is the use of a dynamic decision algorithm in an intelligent system to calculate the greatest number of rooftop solar panels, photovoltaic cells, batteries, floating PV, and solar PV with a grid that can be hybridized and to optimize the residential unit power demand. Figure 1 illustrates the flow diagram of the proposed research.

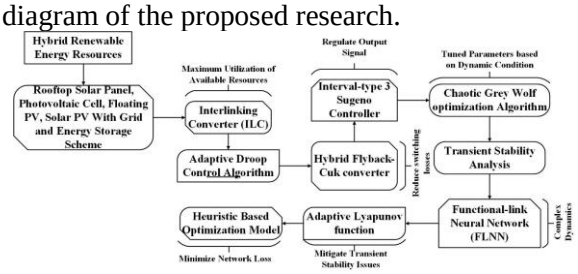

Figure 1. Flow diagram of the proposed research (The authors)

Considering the energy relationship between supply (PV, battery) and load demand, the PV system works in a grid-connected or energy storage scheme, which protects the battery from overcharging. Meanwhile, load-shedding control protects the battery against over-discharging. A simplified and effective control method based on virtual impedance for parallel-connected three-phase DC/AC inverters is presented to achieve power sharing between the battery and SC. The terminal voltage of the SC recovers to its initial value, and the AC bus voltage remains constant during system power changes.

A. Modeling of the AC/DC Microgrid

This research presents a dynamic modeling and control strategy for a sustainable microgrid, principally powered by multiple renewable energy sources, rooftop solar panels, photovoltaic cells, floating PV, solar PV with grid, and an energy storage scheme. Microgrids have become an attractive option for distributed generation (DG) with the increase in renewable energy sources (RES) and storage systems. Furthermore, particularly when paired with renewable generators, batteries provide reliable and cheaper electricity in isolated grids and off-grid communities. Vanadium redox flow battery (VRFB) storage is adopted for peak shaving and microgrid performance reliability as a long-life and scalable battery storage solution.

1) PV System Model

This study uses the PV model shown in Figure 2 because it is suitable for simulating practical PV systems that are composed of numerous PV modules and because it only requires a few parameters, such as the number of PV modules, PV array open-circuit voltage, and short-circuit current. Moreover, this model can represent solar irradiance and temperature changes that may occur commonly during the day. The rated power of the PV system in this study is 10 kW, which comprises 50 KC200GT modules manufactured by Kyocera Solar Energy Inc. The simulated PV system configuration is an array of 5x10 modules, and its voltage and current at the MPP with a solar irradiance of $1\,kW/m^2$ are 261.3 V and 38.1 A, respectively.

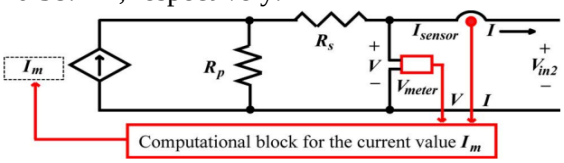

Figure 2. Circuit-based PV model (The authors)

In this study, the hybrid renewable energy resources used comprise rooftop solar panels, photovoltaic cells, floating PV, and solar PV.

These hybrid renewable energy resources are connected to a grid and an energy storage scheme. These solar PV modules are mounted on different places such as land, the surface of water, and the roof of buildings and convert sunlight into direct current. The size of a solar PV system depends on the 90% energy consumption of the building and the shade-free rooftop area available. To achieve the required voltage and current, a group of PV modules is wired into a large array called a PV array.

2) Solar PV Array Support Structure

Solar PV systems use galvanized steel structures to securely mount solar panels on different surfaces such as the ground, water surface, and building roofs. Proper mounting is crucial to maximize power generation. The solar grid inverter plays a key role in converting the generated direct current into alternating current, which is essential for powering electrical appliances. It also regulates battery charging when necessary. The balance of the system includes various components such as cables, junction boxes, and fuses required for the smooth functioning of solar rooftop power plants.

The size of the solar plant depends on factors such as electrical load requirements, kWh consumption, and desired returns. The available shaded-free rooftop space limits the size of the solar plant. The expected lifespan of a solar PV plant is approximately 25 years. Energy storage technology falls into two categories: indirect energy storage, which involves converting electric energy to other forms such as kinetic energy, and direct energy storage, where energy is stored in electric or magnetic fields. These technologies play a vital role in managing and storing excess energy for later use.

3) Modeling of the VRFB Storage

Some of the major advantages of VRFB storage over other conventional batteries are its highest cycle life of approximately 13 000 (≈20 years which is close to the life of solar PV power plants) and the scalability of its power and energy capacity. Thus, VRFB is a suitable storage solution for stationary renewable energy applications to ensure energy system reliability.

The main parameters considered when sizing the battery bank are the charge–discharge characteristics, operating temperature, and variations in solar and wind power. The battery voltage can be expressed in terms of the battery state of charge (SOC), specific resistance, and flow rate.

$$V_{bat} = V_{stack}\left(SOC, Q, n_{cell}\right) \pm I_{stack} * R_{specific}\left(I_{stack}, Q, T\right) \quad (1)$$

where $V_{stack} = VRFB$ stack open-circuit voltage (V), $I_{stack} = VRFB$ stack terminal current (A), $R_{specific}$ is the specific resistance of stack $(m\Omega)$, Q - electrolyte flow rate (mLs^{-1}), and T is the operating temperature $(°C)$. Again, the VRFB SOC is calculated by

$$SOC = \frac{c(t)}{C_{\mathrm{Re}f}}, \quad (2)$$

where $C(t)$ is the battery capacity (Ah) at time instant t; $C_{\mathrm{Re}f}$ is the reference capacity (Ah). Now, $C(t)$ is calculated as

$$C(t) = q(t_0) + q_c(t) + q_d(t) \quad (3)$$

where $q(t_0)$ is the initial quantity of charge (Coulomb), $q_c(t)$ is the charge-in during the charging process (Coulomb), and $q_d(t)$ is the charge-out during the discharging process (Coulomb).

The state of health (SOH) of the battery is defined by

$$SOH = \frac{C_{Ref}(t)}{C_{Ref\_nom}}, \quad (4)$$

where C_{Ref_nom} is the nominal capacity of the reference available.

The new capacity reference C_{Ref} is determined by

$$C_{Ref}(t) = C_{\mathrm{Re}f}(t - \Delta t) - \Delta C_{\mathrm{Re}f}(t) \quad (5)$$

The capacity loss is calculated by

$$-\Delta C_{\mathrm{Re}f}(t) = C_{\mathrm{Re}f\_nom} * Z * \left(SOC(t - \Delta t) - SOC(t)\right) \quad (6)$$

Now the SOH can be expressed as

$$SOH(t) = \frac{C_{\mathrm{Re}f}(t - \Delta t)}{C_{\mathrm{Re}f\_nom}} - Z * \left(SOC(t - \Delta t) - SOC(t)\right) \quad (7)$$

where Z is the linear aging coefficient.

The technical specifications for validating the VRFB system model are shown in Table 1.

Table 1.
Technical specifications for the VRFB storage system (The authors)

Parameters	Values
Number of series cells (n) in a stack	20

Continuation of Table 1	
Volume of Electrolyte in Each Tank	180 L
Power Capacity	1 kW
Energy Capacity	6 kWh
Voltage Range	20–32 V
Maximum Allowable Terminal Current	60 A
VRFB Equilibrium Potential	28 V
Rated Ah Capacity	187 Ah
Stack Temperature Variation	29–31ºC
Pump-Rated Power (x2)	130 W
Charge Controller Efficiency (DC-DC)	96%

Furthermore, to interface the VRFB storage system with the microgrid, a comprehensive electrical equivalent circuit model is used.

$$E_{stack(OCV)}(t) = n \times \left\{ \begin{array}{l} E_{cell\_eq(at\,50\%\,SOC)} + \dfrac{2RT}{F} \\ \times \ln\left(\dfrac{SOC}{1-SOC}\right) - \\ I_d R_{self\_discharge}(t) \end{array} \right\} \quad (8)$$

where $E_{stack(OCV)} = VRFB$ stack open-circuit voltage (V), $E_{Cell\_eq(at\,50\%SOC)} = VRFB$ cell equilibrium potential (V), $n = no.of\ series\ cells\ in\ VRFB\ Stack$, R is the universal gas constant (8.3144 J K^{-1} mol^{-1}), T is the ambient temperature (K), F - Faraday's constant (96 485 C mol^{-1}), I_d is the diffusion current (A), and $R_{self\_discharge}$ is the self-discharge equivalent resistance (Ω). The VRFB stack terminal voltage is estimated using equation (9).

$$E_t(t) = E_{stack(OCV)}(t) \pm I_{stack} R_{\text{int}}(Q, I_{stack}) \quad (9)$$

where $E_t(t) = VRFB$ stack terminal voltage (V), $I_{stack} = VRFB$ stack terminal current (A), $R_{\text{int}} = VRFB$ stack internal resistance (Ω), and Q is the electrolyte flow rate (mLs^{-1}).

An efficient DC converter and inverter for VRFB were used in this work for its interfacing with solar PV, load, and the distribution grid.

B. Converters

The concept of hybrid AC/DC microgrids, comprising both AC and DC grids interconnected by an interlinking converter (ILC), has emerged with the presence of both AC and DC microgrids. In large interconnected microgrids, voltage source converters (VSCs) use non-communication-based droop control to share power demand based on their droop coefficients. However, the constant droop ratio limits the power delivery capacity of the VSCs, even when surplus power is available in their sources. To address this issue, an adaptive droop control algorithm is proposed that dynamically adjusts the droop coefficients of VSCs for optimal resource utilization in each microgrid under various operating modes. In addition, a hybrid flyback-Cuk converter is employed to reduce switching losses and improve the duty cycle range, enhancing voltage step-down efficiency.

1) Adaptive Droop Control Algorithm

The proposed droop-controlled VSC system aims to optimize power use in DCMG1 and DCMG2. When DCMG1 experiences a power deficit but surplus power is available in DCMG2, a constant droop ratio restricts power output from the VSCs, leading to inefficient utilization. To address this, an adaptive droop control method is suggested, which dynamically allocates droop coefficients to VSC-3 and VSC-4 based on the instantaneous load demand of the system. This approach allows for maximum utilization of resources in DCMG1 and DCMG2, ensuring efficient power distribution in the system.

Any change in the load of the system causes a change in the RMS voltage (V_{rms}) at PCC2. The measurement V_{rms} is compared to the reference V^*rms (415 V), and the error is fed to a PI controller to generate a new instantaneous droop coefficient (m_{j2}) of VSC-4. The product of m_{j2} and the previously measured VSC-4 output (P_{VSC-4}) gives the instantaneous frequency deviation (ω_j).

The q-axis component of the reference 3-phase voltage V^*abc is fed to a PI controller to generate the reference frequency ω. The difference between ω and ω_j is integrated to produce the new value θ. This new magnitude θ is used to transform reference voltage V^*abc and measured current (I_L) to their respective dq-axis components $(V^*d, V^*q, and\ I_d,)$. The control of 3-phase voltages (V_{abc}) and currents (I_L) is identical to that of a conventional $V-f$ controller which determines the gate pulses of VSC-4 using the sine pulse width modulation (SPWM) technique.

C. VDC-Q Controlled VSC

The VSC-5 controls the reactive power flow of ACMG1 and maintains the voltage (VDC)

across the capacitor (CDC) within ± 5% of its rated value of 750 V. The measured voltage VDC is compared with the reference voltage magnitude, and the error signal is fed to the PI controller. The remaining part of this VDC Q-controlled VSC has a structure similar to that of the P-Q controlled VSC to generate gate pulses using the SPWM technique.

1) Hybrid Flyback-Cuk Converter

The proposed HFC consists of two converters. The first is the flyback converter, and the second is the Cuk converter. Both converters share the same input components (DC power supply, the primary side of the transformer, and the switch Q). The output of each separate converter is connected in series. Therefore, the output voltage across the load is the difference between the flyback and Cuk output voltages. The proposed converter is controlled by a voltage control loop (PI controller). The controller output produces the relative duty cycle to control the switch Q.

The analysis of the proposed HFC converter can be discussed on the basis of the following assumptions.

1) In the steady state, the average inductor voltage is zero.

2) In the steady state, the average capacitor current is zero.

3) In the steady state, the average value of the Cuk coupling capacitor (C_k) is $V_{in}+V_{out}$.

Two operation modes of the proposed HFC converter are considered according to the state of the switch Q, whether it is ON or OFF. These two modes are.

The Q is ON when both the flyback output diode (D_f) and the Cuk diode (D_k) are reverse biased. During this period, the magnetization inductance (L_m) is energized from the input voltage source. Therefore, the rate of change of current in the magnetization inductance is linearly increased according to the following equation

$$\frac{dI_{L_m}}{dt}=\frac{v_{in}}{L_m} \tag{10}$$

The voltage across the inductor L_k is, $(V_{ck}-V_o)$ and the rate of change of its current is given by

$$\frac{dI_{L_k}}{dt}=\frac{(V_{ck}-v_o)}{L_k} \tag{11}$$

where V_{ck} is the Cuk stage output voltage, as given below in equation (12).

$$V_{ck}=-V_{in}\frac{D_Q}{(1-D_Q)} \tag{12}$$

Diodes (D_f) and (D_k) are conducting. During this mode, L_m is de-energized $(-V_1)$. The rate of change of current in the magnetization inductance is given by:

$$\frac{dI_{L_m}}{dt}=\frac{-v_1}{L_m} \tag{13}$$

Moreover, L_k is also de-energized by the voltage V_{ck}, and the rate of change of the current in the inductor L_k is given by

$$\frac{dI_{L_k}}{dt}=\frac{-v_{ck}}{L_m} \tag{14}$$

From equations (10) to (14), it can be observed that the rate of change in all inductor currents depends on the input/output voltages and inductor values. The duty cycle of the proposed HFC converter (D_Q) can be calculated as

$$V_o=V_f-V_{ck} \tag{15}$$

$$V_o=\frac{N_s}{N_p}V_{in}\frac{D_Q}{1-D_Q}-\frac{D_Q}{1-D_Q}V_{in} \tag{16}$$

Using Equations (15) and (16), we obtain

$$D_Q=\frac{N_pV_o}{N_pV_o+V_{in}(N_s-N_p)} \tag{17}$$

From equation (16), the voltage gain of the proposed HFC converter can be derived as.

$$VG_{HFC}=\frac{V_o}{V_{in}}=\left|\frac{N_s-N_p}{N_p}\frac{D_Q}{1-D_Q}\right| \tag{18}$$

From equation (18), it can be seen (if $N_s<N_p$) that the HFC is a step-down converter.

Moreover, to ensure the step-down functionality of the HFC converter, the voltage gain must be less than 1, i.e., $\frac{V_o}{V_{in}}<1$. The HFC converter is operated in step-down conditions for a duty cycle of up to 82%. While both flyback and Cuk converters are operated in step-down conditions at limited duty cycle values lower than $D=50\%$ then for $D>50\%$, the voltage gain increases dramatically, and the output voltage is increased.

D. Controller

The output of each converter is connected in series. To control the output voltage in the

converter, hybrid techniques are proposed. Recently, interval-type 3 fuzzy systems have begun to appear in different research areas. This research outlines a methodology for the parameterization of interval type-3 membership functions using vertical cuts applied to the dynamic parameter adaptation of the differential evolution algorithm and implemented in a hybrid interval-type 3 Sugeno controller that functions to regulate the output signal by obtaining the duty cycle value. This methodology was applied to the dynamic adaptation of the parameter in differential evolution to improve the performance of this method as generations occur. The Chaotic Grey Wolf Optimization Algorithm tuned Fuzzy type-3 controllers under dynamic conditions, i.e., sudden irradiation variations, deep voltage sag/swell, etc.

1) Interval-Type 3 Sugeno Controller

The differential evolution (DE) algorithm has found various applications in different disciplines, including minimizing agency and user costs, optimizing traffic interruption duration and environmental impact, and enhancing the performance of solar systems through precise cell parameter modeling. Additionally, the DE algorithm has been adapted to solve customer scheduling problems, achieving minimized total completion time with favorable results. In this experiment, a fuzzy system called IT3FDE, which uses the interval type-3 fuzzy system, is employed. The IT3FDE algorithm has an input representing the generations and an output F corresponding to the mutation parameter. The system follows the Mamdani type and consists of three T3 membership functions and three rules. The ScaleTriScaleGaussT3MF membership function is used in the fuzzy system, expressed by equation (19). The results of this approach have shown promising outcomes.

$$\tilde{u}_A(x,u) = Scale\ Triscale Guass\ T3MF \left(X,\{\{[a_1,b_1,c_1]\},\lambda,[l_1,l_2]\}\right) \tag{19}$$

The interval type-3 triangular membership function, $\tilde{u}_A(x,u) = Scale\ Triscale Guass\ T3MF$, with triangular $FOU(A)$ is characterized by parameters $[a_1,b_1,c_1]$ (UpperParameters) for the upper membership function (UMF) and λ (LowerScale), l (LowerLag) for the lower membership function (LMF), to form the domain of uncertainty (DOU) with parameters $DOU = \left[\underline{\mu}(x), \bar{\mu}(x)\right]$. The vertical slices $A_{(x)}(u)$ characterize the $FOU(A)$ these are IT2-FSs with Gaussian T2 MF, $\mu_{A(x)}(u)$ with parameters $[\sigma_u, m(x)]$ for the UMF and LMF λ (LowerScale), λ (LowerLag). The $\tilde{u}_A(x,u) = Scale\ Triscale Guass\ T3MF$ is described by $\left(X,\{\{[a_1,b_1,c_1]\},\lambda,[l_1,l_2]\}\right)$ equations (20) and (21).

$$\bar{\mu}(x) = \begin{cases} 0 & x < a_1 \\ \dfrac{x-a_1}{b_1-a_1} & a_1 \le x \le b \\ \dfrac{c_1-x}{c_1-b_1} & b_1 \le x \le c_1 \\ 0 & x > c_1 \end{cases} \tag{20}$$

where $a_2 = b_1 - (b_1 - a_1)(1-l_1)$ and $c_2 = b_1 - (c_1 - b_1)(1-l_2)$.

$$\bar{\mu}(x) = \begin{cases} 0 & x < a_1 \\ \dfrac{x-a_2}{b_1-a_2} & a_2 \le x \le b \\ \dfrac{c_2-x}{c_2-b_1} & b_1 \le x \le c_2 \\ 0 & x > c_2 \end{cases} \tag{21}$$

The function $\mu(x)$ is multiplied by the parameter λ to form the LMF of the DOU, $\underline{\mu}(x)$, described as $\underline{\mu}(x) = \lambda\mu(x)$. Then, $\bar{\mu}(x)$ and $\underline{\mu}(x)$ are the upper and lower DOU limits. The range, $\delta(u)$ and radius, σ_u of the FOU are defined in equations (22) to (24).

$$\delta(u) = \underline{\mu}(x) - \bar{\mu}(x) \tag{22}$$

$$\sigma_u = \frac{\delta(u)}{2\sqrt{3}} + \varepsilon \tag{23}$$

The apex or core $m(x)$, of the T3 MF $\tilde{u}(x,u)$ is defined by equations.

$$m(x) = \begin{cases} 0 & x < a \\ \dfrac{x-a}{b_1-a} & a \le x \le b_1 \\ \dfrac{c-x}{c-b_1} & b_1 \le x \le c \\ 0 & x > c \end{cases} \tag{24}$$

where $a = (a_1 + a_2)/2$ and $c = (c_1 + c_2)/2$. Then, vertical cuts with T2 MF

$\mu_{A(x)}(u) = \left[\underline{\mu}_{A(x)}(u), \bar{\mu}_{A(x)}(u)\right]$

They are described by equations (25) and (26).

$$\tilde{u}_{A(x)}(u) = \exp\left[-\frac{1}{2}\left(\frac{u-m(x)}{\sigma_u}\right)^2\right] \tag{25}$$

$$\bar{\mu}_{A(x)}(u) = \lambda.\exp\left[-\frac{1}{2}\left(\frac{u-m(x)}{\sigma^*_u}\right)^2\right] \quad (26)$$

where $\sigma^*_u = \sigma_u\sqrt{\frac{\ln(l)}{\ln(\varepsilon)}}$ and $l = (l_1 + l_2)/2$. Supposing $l = 0$. Then, $\sigma^*_u = \sigma_u$. Accordingly, $\bar{\mu}_{A(x)}(u)$ and $\underline{\mu}_{\mathbb{A}(x)}(u)$ $\underline{\mu}_{A(x)}(u)$ are the UMF and LMF of the IT2-FSs of the vertical cuts.

2) Chaotic Grey Wolf Optimization Technique

Chaos theory is introduced into the GWO algorithm to accelerate its global convergence speed. Despite having a reasonable convergence rate, GWO has low solving accuracy and poor local searchability. To overcome the shortcomings of GWO, the CGWO algorithm is developed by introducing a piecewise chaotic map in the GWO algorithm to produce a diverse initial population with uniform distribution as per (27). The reader may refer to additional information and paradigms. Local minima stagnation is avoided by chaos, randomness, and ergodicity.

$$\bar{\mu}(x) = \begin{cases} p_k & 0 \le p_k \le a \\ \frac{p_k - a}{0.5 - a_1} & a_1 \le p_k \le 0.5 \\ \frac{1-a-p_k}{0.5-a} & 0.5 \le p_k \le 1-a \\ \frac{1-a-p_k}{0.5-a} & 1-a \le p_k \le 1 \end{cases} \quad (27)$$

The exact hierarchy of wolves in a wolf pack is considered GWO, which is α, β, γ, and ζ. The roles and responsibilities of the wolves in the group are reduced in descending order. The α wolf is a pack leader responsible for giving instructions and making decisions. β Wolf is the second to command and the best candidate to replace α. γ wolves take order from α, β and dominate ζ, which is the fourth and last level. ζ Wolves maintain safety and integrity in their pack.

The first step of CGWO is to generate a diverse population with uniform distribution start of wolf packs. The chaotic map described in (27) is mapped using the iterative algorithm to initialize the first chaotic numbers. Various parameters involved in the CGWO algorithm for conducting the exploration–exploitation mechanism viz. 'a', 'A' and 'C' are generated, the same as in GWO (28)-(30). The distances from α, β, and γ wolves, i.e., D_α, D_β, and D_γ to each of the remaining wolves ($\vec{p}$) as a fitness function, using the effect of α, β and γ wolves on the prey viz. $\overrightarrow{p_1}$, $\overrightarrow{p_2}$, and $\overrightarrow{p_3}$ can be calculated further. The fitness of an initialized population of the wolf in the search space is calculated and sorted using the introduced chaotic map and is sorted according to their fitness. The fittest wolf position will be updated in the next iteration (31) and the wolf's position may be obtained as' the optimal solution in case termination criteria are fulfilled. In each iteration, the associated parameter values are also updated (30).

$$\overrightarrow{D_\alpha} = \left|\overrightarrow{C_1} \times \overrightarrow{p_\alpha} - \vec{p}\right|, \overrightarrow{D_\beta} = \left|\overrightarrow{C_2} \times \overrightarrow{p_\beta} - \vec{p}\right|, \overrightarrow{D_\gamma} = \left|\overrightarrow{C_3} \times \overrightarrow{p_\gamma} - \vec{p}\right| \quad (28)$$

$$\vec{p}(t+1) = \left(\overrightarrow{p_1} + \overrightarrow{p_2} + \overrightarrow{p_3}\right)/3 \quad (29)$$

With termination, criteria that satisfy the leader wolf's fitness or position will be considered the most optimal solution or PI controller gains for V_{dc} and V_{pcc} regulation by the CGWO algorithm.

E. Transient Stability

To address the transient power angle stability problem caused by DC line grounding faults in AC/DC interconnected systems, a novel transient stability analysis method based on the stability margin of dynamic energy is proposed. To improve the reliability and robustness of machine learning models forecasting power system transient stability, this study integrates power system dynamics into the data-gathering process. Using recurrent neural networks (RNNs) for multivariate applications, especially in systems with complex and uncertain dynamics, this study enhances the RNN' performance by incorporating functional-link neural networks (FLNNs). In addition, an adaptive Lyapunov function method is proposed to mitigate transient stability issues in RES-connected systems. Furthermore, this study establishes a heuristic-based optimization model for maximizing renewable energy penetration capacity and minimizing network loss, considering transient stability constraints in AC-DC hybrid grids. These methods contribute to more secure and efficient power systems with increased renewable energy integration.

1) Functional-Link Neural Network

FLNNs are a subset of HONNs that do not have any hidden neurons, and the additional neurons are functions of the original features. FLNN enhances N dimension space of the original features to $(n+1)N$ dimension space by mapping each original feature x , to $n+1$ secondary features using the expansion functions.

$$\varphi(x) = [\varphi_0(x), \varphi_1(x), \varphi_2(x), \ldots \varphi_n(x)] \quad (32)$$

Enhancing the features using polynomials to a certain degree is effective for solving many

classification problems. In general, enhancing the d dimensional inputs up to degree r will result in $(d+r)!/d!r!$ polynomials.

For most real-life problems, degrees higher than 3 are too large and increase the risk of overfitting. As such, in this study, we will consider terms up to the degree of 2. The network output function is calculated as

$$y_k = \sum_{i=1}^{d'} w_{ik}\varphi_i(x) \tag{33}$$

where y_k is the output of the k^{th} output node, w_{ik} is the weight of the connection from i^{th} input node to the k^{th} output node and d' is the dimension of the enhanced space. The $\varphi_i(x)$ are polynomial terms constructed out of the novel feature. For example, for a 2-dimensional problem x_1, x_2 the expanded feature space to a degree of 2 can be given as follows:

$$\left[x_1, x_2, x_1^2, x_1, x_2, x_2^2\right] \tag{34}$$

The linear input-output mapping in the new space is not linear in the original space. As a result, quadratic error minimization leads to the following weight updating formula,

$$\Delta\omega_i = \mu\left(y-y\right)\varphi_i(x) \tag{35}$$

where μ is the learning rate. In this study, network training was terminated after 1000 epochs. A set of weights that resulted in the least validation error was selected as the final weights of the trained network. After completion of the learning process, the trained FLNN model was used to test the unseen data.

2) Heuristic-Based Optimization

Due to the renewable energy resource volume and geographical location constraints, the capacity of renewable energy that can be integrated into each access location has an upper limit:

$$C_{DG}^i \le \left[C_{DG}^i\right]^M \quad i \in \Omega_{DG} \tag{36}$$

where C_{DG}^i is the maximum allowable renewable energy capacity integrated into node i.

The renewable energy penetration capacity evaluation model of the AC-DC hybrid grid presents a challenging nonlinear mixed-integer programing problem, making direct analytical solutions impractical. To overcome this, a heuristic solution method is proposed in this section, focusing on the typical operation mode of the power grid and simplifying factors such as load fluctuation and network structure changes. The method is divided into two steps: first, determining the maximum renewable energy penetration capacity that meets transient frequency stability constraints and second, identifying the optimal access location for renewable energy. The chosen access scheme with the minimum system network loss is the optimal solution for the model. By following this process, the obtained renewable energy penetration capacity and location satisfy all optimization constraints while maximizing renewable energy integration and minimizing system network loss. This yields the optimal scheme for the renewable energy penetration capacity optimization model, where the capacity of renewable energy represents the renewable energy penetration capacity of the power grid.

V. EXPERIMENTATION RESULTS AND DISCUSSION

Simulation studies were conducted to analyze the effect of changes in load demand and adaptive droop ratio on the stability of a microgrid with two droop-controlled inverters. Furthermore, the performance of the interconnected HMG is also studied for inter- and intra-MG power transfer using constant and adaptive droop ratios. To verify the results, Matlab/Simulink R2020a is used. The selected solver is an ordinary differential equation (ode23 TB) with a relative tolerance of 10^{-3}, and a maximum step size of 25 µs is selected. The simulation time is set to 2 s to ensure that the proposed HFC converter eventually operates at a steady state.

The simulation model for the proposed study is presented in Figure 3. The generated DC voltage from these sources is synchronized to a particular DC voltage (220V approx.) so that one three-phase voltage source PWM generator can be used for the entire system. This AC voltage obtained after filtration is of 200Volts. To operate the MG in grid-connected mode, a three-phase transformer connected in Delta-star configuration is designed, which steps up the 200V AC to 400V, such that power can be fed to the utility grid.

Table 2.
Simulation system configuration (The authors)

MATLAB/Simulink	Version R2020a
Operation System	Windows 10 Home
Memory Capacity	6GB DDR3
Processor	Intel Core i5 @ 3.5GHz
Simulation Time	10.190 seconds

The performance of the proposed method was evaluated using Matlab/Simulink r2020a software. The operating system of the software is

Windows 10 Home; its memory capacity is 6 GB DDR3. It uses an Intel Core i5 @ 3.5GHz processor, and the time taken for simulation is 10.190 seconds depicted in Table 2.

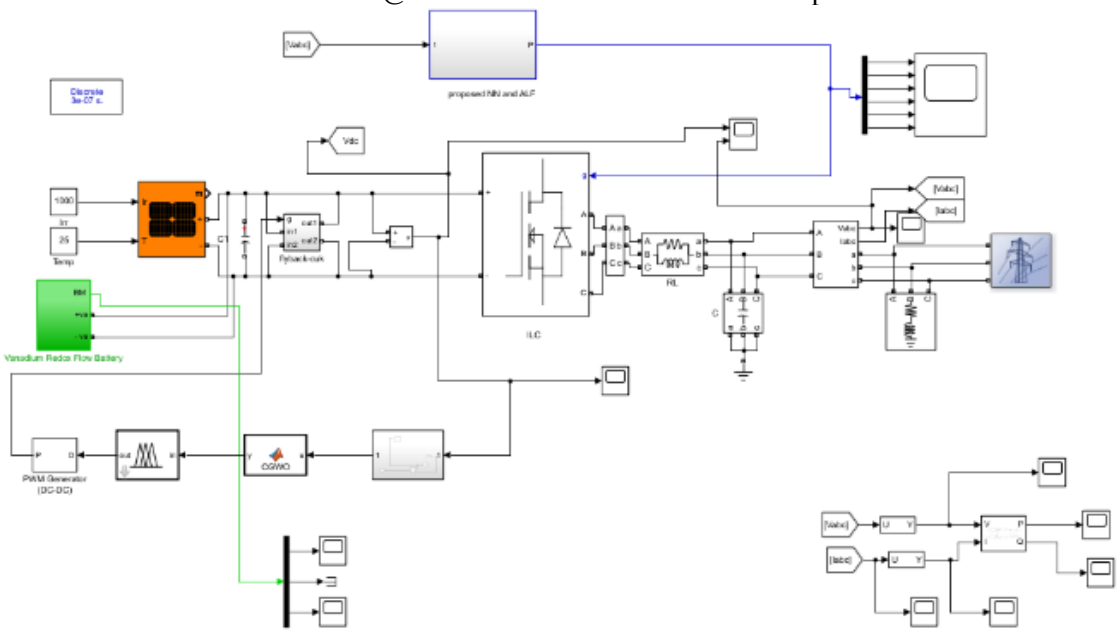

Figure 3. Simulation model for the proposed work (The authors)

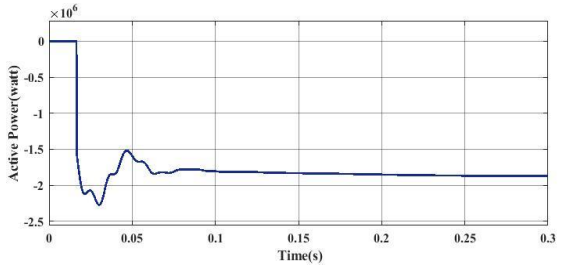

Figure 4. Active power graph (The authors)

Figure 4 illustrates active power sharing in the Microgrid (MG). Each power variation event is evaluated to observe the power-sharing behavior between the voltage source converter (VSCa) and the utility grid under different operating conditions. During event 1 (0.03s), power from the AC source and the interlinking converter (ILC) is injected into the AC microgrid (ACMG), while VSCa and the utility grid absorb this energy. In event 2 (0.03-0.05s), the ILC absorbs power due to the condition of the Direct Current Microgrid (DCMG). However, the AC source still generates excess power, causing VSCa and the utility grid to continue absorbing power. Transitioning to event 3 (0.5–0.1s), AC loads become dominant, requiring VSCa and the grid to inject power into the ACMG. In event 4 (0.1–0.3s), the ILC begins to inject power, but the overall operating condition remains consistent. These observations shed light on the dynamic power flow between VSCa, the utility grid, and the different microgrids in the system.

The reactive power profiles for the AC sources and loads were established to analyze the reactive power influence in the HMG, as presented in Figure 5. These reactive profiles directly affect the power factor at PCC of ACMG. It is perceived that the reactive power is injected into the grid in events 1 and 2; while the reactive power is absorbed in events 3 and 4. However, VSCa is used to perform harmonic mitigation, which reduces the reactive power inherent in harmonic distortion.

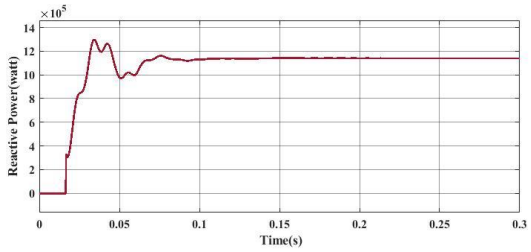

Figure 5. Reactive power graph (The authors)

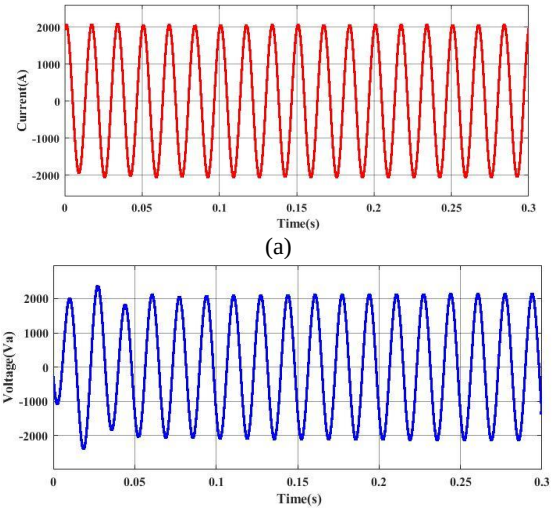

Figure 6. Current and voltage produced by this research (The authors)

Figure 6 reveals that voltage and current instability are related to the optimal filter design parameters. When the results at two different line voltages are taken for the same capacitance value used in the simulation, this value can be changed to obtain more stable signals with minimum ripple percentage values. At a low line voltage (1050 Vrms), after 0.05 s, the voltage and current settled down and became more stable. In addition, the ripple percentage for reverse voltage and current is within the standard limits.

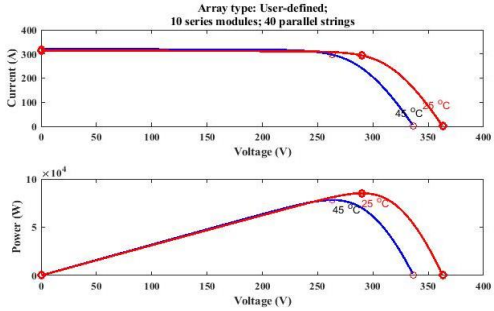

Figure 7. Current and power produced in the PV array (The authors)

Figure 7 shows the control performance of the proposed converter when solar irradiance changes. It represents current and power, and this Figure shows the input and output power of the MI Cuk converter, the PV cells, and the power of the PV modules' Here, the PV array is user-defined, where, and it consists of 10 series modules and 40 parallel strings. There seem to be differences between and due to the switching and conduction losses in the active circuit components.

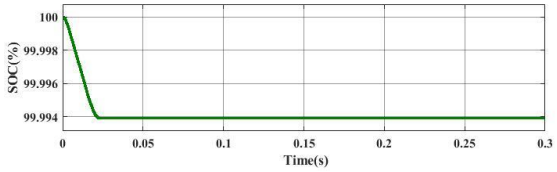

Figure 8. SOC of the battery (The authors)

Figure 8 shows the SOC of the battery. During the entire process, the PV works and the SOC of the battery is always maintained within the preset operation range. The operating results are shown when the SOC of the battery reaches SOC_{max} (99%). Suppose that the solar irradiance is $1000\,W/m^2$ and keeps constant, the initial load power is 40kW and increases to 100kW at $t = 2s$. The battery absorbs excess power at about 40kW and its SOC increases gradually and then reaches its upper limit (90%) at about $t = 0.9s$, the battery cannot be charged continually at this state. The SOC of the proposed work is 99.994%.

The simulation results for the input three-phase and battery voltages are shown in Figure 9. The input three-phase voltage produces approximately 2010 V for the time from 0.05s to 0.3 s. However, the battery voltage is relatively constant until about 0.05 to 0.3 s, which produces a voltage of 220.5V. The voltage goes below 214V when the time is 0.025s.

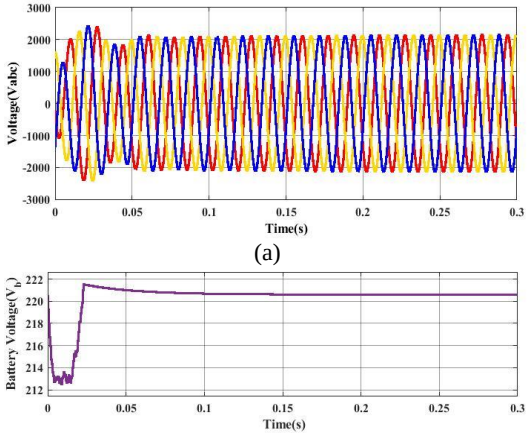

Figure 9. Voltage graph: (a) three-phase voltage; (b) battery voltage (The authors)

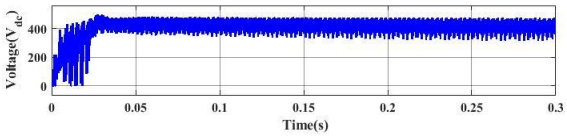

Figure 10. DC voltage graph (The authors)

In Figure 10, the V_{dc} (DC output voltage) is depicted, showing an average output voltage of 400 V DC (green). The 50 V load voltage is the combined result of the flyback and Cuk voltages. Energy transfer from the input to the output occurs through the flyback capacitor. Additionally, the output energy stored in the Cuk capacitor can be used to simultaneously charge a storage element, such as a battery. The dual operation capability of the proposed topology makes it particularly advantageous for innovative power system applications.

A. Transient Frequency Stability Verification

To verify the transient frequency stability of the system under the optimal access scheme of renewable energy, the transient process of the system after power shortage is simulated to verify whether the transient frequency deviation is within the allowable range. Since the renewable energy capacity is greater than the DC unipolar capacity, the power shortage is set as the power shortage caused by the renewable energy trip. Further, 300 and 350 MW of renewable energy are integrated into bus 26, respectively, and the system transient frequency obtained by the simulation is shown in Figure 4.

Figure 11 shows that the renewable energy

penetration capacity is 300 MW, the maximum frequency deviation of the system is less than 1 Hz, and the steady-state frequency deviation is less than 0.2 Hz, satisfying the transient frequency stability constraints. When the renewable energy penetration capacity is 350 MW, the maximum frequency deviation is greater than 1 Hz and exceeds the limit. Correctness of the evaluation results of the renewable energy penetration capacity and effectiveness of the transient frequency stability constraints.

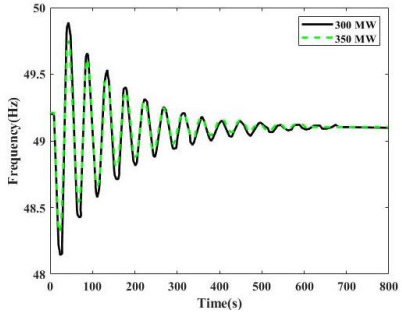

Figure 11. Transient frequency under 300 and 350 MW renewable energy resources (The authors)

Figure 12 illustrates the comparison graph for the voltage conservation ratio. This portrays that the proposed HFCC converter is compared with the existing MIB converter. The voltage conservation ratio is measured when the duty ratio is 0 to 5. However, when compared with these existing methods, high voltage conservation ratio for the proposed converter is 4.9.

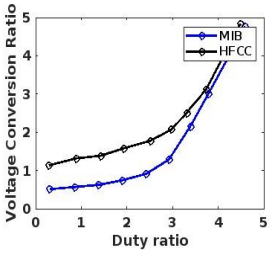

Figure 12. Comparison graph for the voltage conservation ratio (The authors)

Figure 13 shows the tracking performance of the proposed Interval Type-3 -SC converter compared to different existing converters such as Type-1 FLC and Type-2 FL converters and a fixed l. This Figure demonstrates that the output has no obvious change when k is augmented to a certain value.

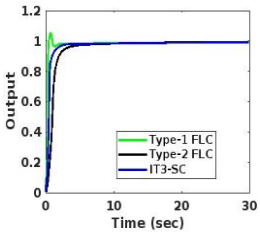

Figure 13. Tracking the performance of the converters (The authors)

The DC bus voltage of the proposed converter is compared with that of the existing fuzzy PID controller in Figure 14. The bus voltage is measured for time seconds, from 0 to 1.5 seconds. The proposed controller reaches 680 V when the time is 0.2 seconds, but it reaches stable values of approximately 5000 V for the time 0.5 to 1.5 seconds.

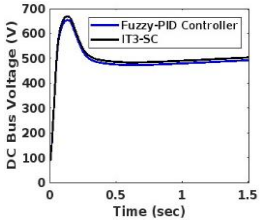

Figure 14. Comparison graph for DC bus voltage (The authors)

Figure 15 shows the comparison graph for controllers, which depicts the peak value, overshoot, undershoot, and settling time of the converters. The proposed technique is compared with existing AFN-FTSC and FTSC controllers. Compared to this existing converter, the proposed controller produces higher performance.

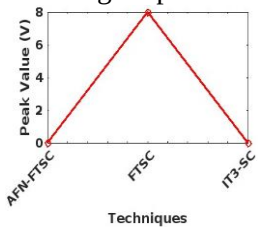

(a) Peak value

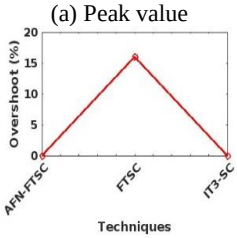

(b) Overshoot

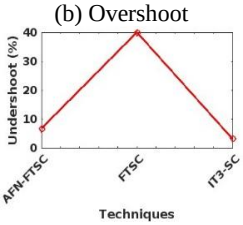

(c) Undershoot

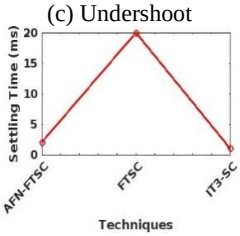

(d) Settling time

Figure 15. Comparison graph for the converters (The authors)

The efficiency graph for the proposed

controller is compared to the existing ALO FOPID and FST FOPID controllers shown in Figure 16. It depicts that the efficiency of the proposed work is evaluated on the basis of the supply voltage. The supply voltage of the proposed work is 50–300 V. When the supply voltage is 50, the efficiency of the work is 91%; however, when the supply voltage is 300, the efficiency of the proposed controller is approximately 95%. This indicates that the efficiency of the proposed method is higher than that of the other existing techniques.

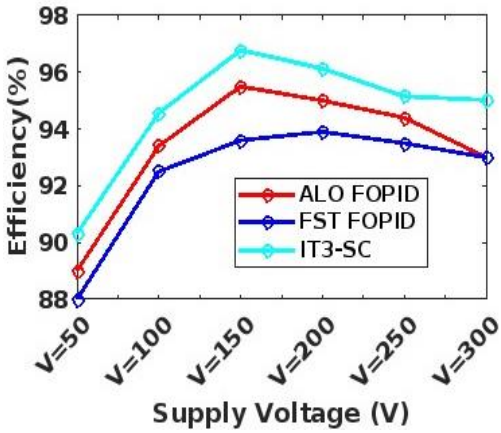

Figure 16. Efficiency graph for controllers (The authors)

The loss calculations and the efficiency of the HFC converter are compared with the efficiency of the existing SRC and high-step-up converter in Figure 17. This Figure shows that the proposed HFCCs have higher efficiency than the other existing methods like 96.7%, but the other two existing methods produce a lower efficiency level.

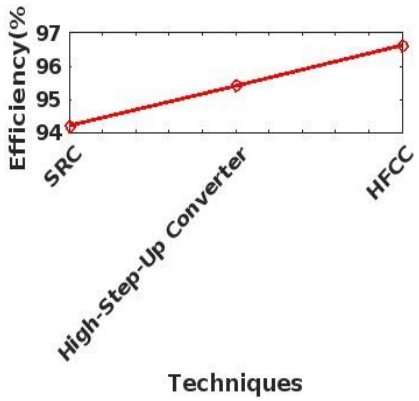

Figure 17. Comparison graph for the converter efficiency (The authors)

Figure 18 displays the voltage gain versus the duty cycle for the flyback Cuk, SRC converters, and the proposed HFCC converter. It can be seen that the HFCC the converter demonstrates lowest voltage gain compared to the other converters. Moreover, to ensure the step-down functionality of the HFC converter, the voltage gain must be less than 1. The HFC converter is operated in step-down conditions for a duty cycle of up to 82%. While both flyback Cuk, and SRC converters are operated in step-down conditions at limited duty cycle values lower than D = 50%, for D > 50%, the voltage gain increases dramatically, and the output voltage is increased.

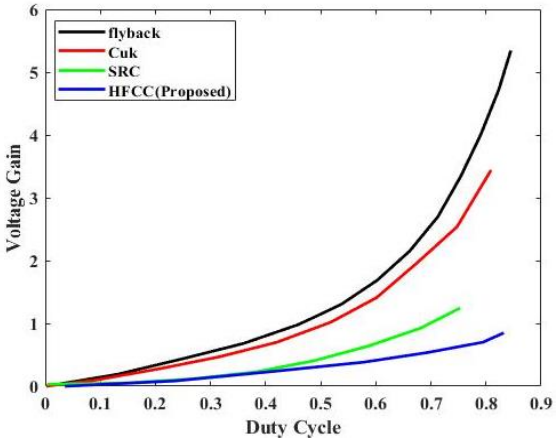

Figure 18. Comparison graph for voltage gain vs. duty cycle (The authors)

VI. CONCLUSION

This study focuses on hybrid renewable energy resources within microgrids and proposes an adaptive droop control algorithm to maximize the utilization of available resources in different operating modes. To overcome certain limitations, a novel hybrid flyback-Cuk (HFC) DC-DC converter with recharging capability is introduced for energy conversion systems. The presented interval-type 3 Sugeno controller regulates the output signal by determining the duty cycle value. A heuristic-based optimization model is also presented to address transient stability constraints. Simulations in a MATLAB/Simulink environment verify the stable and satisfactory operation of the proposed system. This study shows promising results with active and reactive power outputs, voltage profiles, and state of charge (SOC). The proposed work produces active and reactive power is -1.8×10^6 , and 11.5×10^5 , however, the voltage produced in this work is 1050 Vrms. The generated power is 9×10^4 for the voltage is 300, accordingly, the SOC of the proposed work is 99.994%. Accordingly, the performance of the overall control scheme is experimentally validated using a grid-connected hybrid microgrid. The proposed energy management scheme is scalable and suitable for large-scale renewable energy-integrated power systems. By analyzing the impact of access location on transient voltage stability and renewable energy consumption capacity, this research ensures the reliability and effectiveness of microgrid operation. Overall, the adaptive droop controller

implementation is expected to yield significant energy savings over extended periods, making the proposed hybrid microgrid topology valuable for large-scale renewable energy-integrated power systems.

REFERENCES

[1] RADOVANOVIC, A., and MILANOVIC, J.V. (2022) Equivalent modelling of hybrid RES plant for power system transient stability studies. IEEE Transactions on Power Systems, 37(2), pp. 847-859.

[2] HE, P., QI, P., JI, Y., and LI, Z. (2021) Dynamic interactions stability analysis of hybrid renewable energy system with SSSC. Archives of Electrical Engineering, 70(2), pp. 442-465. https://doi.org/10.24425/aee.2021.136995

[3] CAI, W., et al. (2020) Optimal sizing and location based on economic parameters for an off-grid application of a hybrid system with photovoltaic, battery and diesel technology. Energy (Oxf.), 201, 117480.

[4] KUMAR, A., MISHRA, V. M., and RANJAN, R. (2021) Fuzzy Distribution Static Compensator based control strategy to enhance low voltage ride through capability of hybrid renewable energy system. Energy Sources, Part A: Recovery, Utilization, and Environmental Effects, pp. 1-18. https://doi.org/10.1080/15567036.2021.1936696

[5] BASEER, A., ALMUNIF, M., ALSADUNI, A., ZUBAIR, I., and TAZEEN, M. (2022) An adaptive power point tracker in wind photovoltaic system using an optimized deep learning framework, Energy Sources, Part A. Recovery, Utilization, and Environmental Effects, 44, pp. 4846–4861.

[6] MALIK, H., CHAUDHARY, G., and SRIVASTAVA, S. (2022) Digital transformation through advances in artificial intelligence and machine learning. Journal of Intelligent & Fuzzy Systems, 42(2), pp. 615-622.

[7] AL-SHAMMAA, A. A., HUSSEIN FARH, H. M., NOMAN, A. M., AL-SHAALAN, A. M., and ALKUHAYLI, A. (2022) Optimal Sizing of a Hybrid Renewable Photovoltaic-Wind System-Based Microgrid Using Harris Hawk Optimizer. International Journal of Photoenergy, 2022, Article ID 4825411, pp. 1-13. https://doi.org/10.1155/2022/4825411

[8] BOUDIA, A., MESSALTI, S., HARRAG, A., and BOUKHNIFER, M. (2021) New hybrid photovoltaic system connected to superconducting magnetic energy storage controlled by PID-fuzzy controller. Energy Conversion and Management, 244, 114435, https://doi.org/10.1016/j.enconman.2021.114435

[9] YUAN, G., WANG, H., KHAZAEI, E., and KHAN, B. (2021) Collaborative advanced machine learning techniques in optimal energy management of hybrid AC/DC IoT-based microgrids. Ad Hoc Networks, 122, 102657, https://doi.org/10.1016/j.adhoc.2021.102657

[10] JIN J. X., et al. (2022) A superconducting magnetic energy storage based current-type interline dynamic voltage restorer for transient power quality enhancement of composited data center and renewable energy source power system. Journal of Energy Storage, 52(C), 105003, https://doi.org/10.1016/j.est.2022.105003

[11] FAROOQ, Z., RAHMAN, A., and LONE, S. A. (2021) System dynamics and control of EV incorporated deregulated power system using MBO-optimized cascaded ID-PD controller. International Transactions on Electrical Energy Systems, 31(11), e13100, https://doi.org/10.1002/2050-7038.13100

[12] MAHAKUR, A., and MOHANTY, D. (2022) Frequency Control of SPV/Wind/Biogas/Biodiesel-Based Microgrid Using Fuzzy-Aided PID Controllers. Advances in Sustainability Science and Technology, Singapore: Springer Singapore, pp. 611–624.

[13] SAHOO, B. P., and PANDA, S. (2020) Load frequency control of solar photovoltaic/wind/biogas/biodiesel generator based isolated microgrid using Harris hawks optimization. Proceedings of the First International Conference on Power, Control and Computing Technologies (ICPC2T), Raipur, India, 2020, pp. 188-193,

https://doi.org/10.1109/ICPC2T48082.2020.9071507.
[14] JOY, J. S., UDDIN, N., ISLAM, M. S., and ISLAM, M. T. (2021) An innovative method to hybrid renewable energy controlling strategy using artificial techniques. International Journal of Mechanical Engineering and Robotics Research, 10(3), pp. 137-150.
[15] MAQBOOL, H., et al. (2022) An optimized fuzzy based control solution for frequency oscillation reduction in electric grids. Energies, 15(19), 6981.
[16] SURESH, M., MEENAKUMARI, R., PANCHAL, H., PRIYA, V., EL AGOUZ, E. S., and ISRAR, M. (2022) An enhanced multiobjective particle swarm optimisation algorithm for optimum utilisation of hybrid renewable energy systems. Internatonal Journal of Ambient Energy, 43(1), pp. 2540-2548.
[17] YAN, R., et al. (2022) A two-stage stochastic-robust optimization for a hybrid renewable energy CCHP system considering multiple scenario-interval uncertainties. Energy (Oxf.), 247, 123498.
[18] SEDAGHATI, A., and AL-DURRA, A. (2023) Saturated full model capability of virtual synchronous generator to improve transient stability of hybrid power system, IET Renewable Power Generation, 17(1), pp. 52-65.
[19] HOBALLAH, A., EL-SAYED, S. K., AL OTAIBI, S., HENDAWI, E., ELKALASHY, N., and AHMED, Y. (2022) Risk assessment of power system transient instability incorporating renewable energy sources. International Journal of Electrical and Computer Engineering, 12(5), pp. 4649-4660. https://doi.org/10.11591/ijece.v12i5.pp4649-4660
[20] AGARALA, A., BHAT, S. S., MITRA, A., ZYCHMA, D., and SOWA, P. (2022) Transient stability analysis of a multi-machine power system integrated with renewables. Energies, 15(13), 4824.
[21] KRISHNAN, V. A., and KUMAR, N. S. (2022) Robust Soft Computing Control Algorithm for Sustainable Enhancement of Renewable Energy Sources based Microgrid. A Hybrid Garra Rufa Fish Optimization-Isolation Forest Approach. Sustainable Computing: Informatics and Systems, 35, 100764, https://doi.org/10.1016/j.suscom.2022.100764
[22] KUMAR, R., DIWANIA, S., SINGH, R., ASHFAQ, H., KHETRAPAL, P., and SINGH, S. (2022) An intelligent Hybrid Wind-PV farm as a static compensator for overall stability and control of multimachine power system. ISA Transactions, 123, pp. 286-302.
[23] LI, C., et al. (2022) An evaluation method of renewable energy resources' penetration capacity of an AC-DC hybrid grid. Energies, 15(7), 2550. https://doi.org/10.3390/en15072550
[24] AMINE, H. M., MESSAOUD, H., OTHMANE, A., SAAD, M., ABDALLAH, B., and OUSSAMA, H. (2021) Energy Management Strategy of an Isolated DC-Microgrid Adopting Photovoltaic and Hybrid Energy Storage System, Assessment of Solar Condition Impact. In OUAISSA, M., OUAISSA, M., EL HIMER, S., & BOULOUARD, Z. (Eds.) Advances in Communication Technology, Computing and Engineering, pp. 875-887.

参考文：

[1] RADOVANOVIC, A. 和 MILANOVIC, J.V. (2022) 用于电力系统暂态稳定性研究的混合 RES 电站的等效建模。IEEE 电力系统汇刊，37(2)，第 847-859 页。
[2] HE, P., QI, P., JI, Y., 和 LI, Z. (2021) 混合可再生能源系统与 SSSC 的动态相互作用稳定性分析。电气工程档案，70(2)，第 442-465 页。https://doi.org/10.24425/aee.2021.136995
[3] CAI, W., 等。(2020) 基于经济参数的最佳尺寸和位置，用于采用光伏、电池和柴油技术的混合系统的离网应用。能源（牛津），201, 117480。
[4] KUMAR, A.、MISHRA, V. M. 和 RANJAN, R. (2021) 基于模糊分布静态补偿器的控制策略，增强混合可再生能源系统的低电压穿越能力。能源，A 部分：回收、利用和环境影响，第 1-18 页。

https://doi.org/10.1080/15567036.2021.1936696
[5] BASEER, A. 、 ALMUNIF, M. 、 ALSADUNI, A.、ZUBAIR, I. 和 TAZEEN, M. (2022) 使用优化深度学习框架的风电光伏系统自适应功率点跟踪器，能源，A 部分：回收、利用和环境影响，44，第 4846–4861 页。
[6] MALIK, H.、CHAUDHARY, G. 和 SRIVASTAVA, S. (2022) 通过人工智能和机器学习的进步实现数字化转型。智能与模糊系统杂志，42(2)，第 615-622 页.
[7] AL-SHAMMAA, A. A. 、 HUSSEIN FARH, H. M.、NOMAN, A. M.、AL-SHAALAN, A. M. 和 ALKUHAYLI, A. (2022) 使用哈里斯霍克优化器优化基于混合可再生光伏风电系统的微电网的规模。国际光能杂志，2022，文章 ID 4825411，第 1-13 页。https://doi.org/10.1155/2022/4825411
[8] BOUDIA, A. 、 MESSALTI, S. 、 HARRAG, A. 和 BOUKHNIFER, M. (2021) 连接到由 PID 模糊控制器控制的超导磁储能的新型混合光伏系统。能源转换与管理，244, 114435，https://doi.org/10.1016/j.enconman.2021.114435
[9] YUAN, G.、WANG, H.、KHAZAEI, E. 和 KHAN, B. (2021) 基于混合交流/直流物联网的微电网优化能源管理的协作先进机器学习技术。自组织网络，122, 102657，https://doi.org/10.1016/j.adhoc.2021.102657
[10] JIN, J. X.，等。(2022) 一种基于超导磁储能的电流型线间动态电压恢复器，用于增强复合数据中心和可再生能源电力系统的瞬态电能质量。储能杂志，52(C)，105003，https://doi.org/10.1016/j.est.2022.105003
[11] FAROOQ, Z. 、 RAHMAN, A. 和 LONE, S. A. (2021) 使用管理层收购优化的级联 ID-PD 控制器对电动汽车并入解除管制的电力系统进行系统动力学和控制。国际电能系统交易，31(11)，e13100，https://doi.org/10.1002/2050-7038.13100
[12] MAHAKUR, A.，和 MOHANTY, D. (2022) 使用模糊辅助 PID 控制器对基于特殊病毒/风能/沼气/生物柴油的微电网进行频率控制。可持续发展科学与技术进展，新加坡：施普林格新加坡，第 611-624 页.
[13] SAHOO, B. P. 和 PANDA, S. (2020) 使用哈里斯鹰队优化对基于太阳能光伏/风能/沼气/生物柴油发电机的隔离微电网进行负载频率控制。第一届国际电力、控制和计算技术会议(ICPC2T)会议记录，印度赖布尔，2020，第 188-193 页，https://doi.org/10.1109/ICPC2T48082.2020.9071507。
[14] JOY, J. S., UDDIN, N., ISLAM, M. S.，和 ISLAM, M. T. (2021) 使用人工技术的混合可再生能源控制策略的创新方法。国际机械工程和机器人研究杂志，10(3)，第 137-150 页。
[15] MAQBOOL，H.，等。(2022) 用于减少电网频率振荡的优化模糊控制解决方案。能源，15（19），6981。
[16] SURESH, M., MEENAKUMARI, R., PANCHAL, H., PRIYA, V.，等。(2022) 用于优化利用混合可再生能源的增强型多目标粒子群优化算法 系统。国际环境能源杂志，43(1)，第 2540-2548 页。
[17] YAN, R.，等。 (2022) 考虑多场景间隔不确定性的混合可再生能源冷热电联供系统的两阶段随机鲁棒优化。能源（牛津），247, 123498。
[18] SEDAGHATI, A. 和 AL-DURRA, A. (2023) 虚拟同步发电机的饱和全模型能力以提高混合电力系统的暂态稳定性，IET 可再生发电，17(1)，第 52–65 页 。
[19] HOBALLAH, A.、EL-SAYED, S. K.、AL OTAIBI, S.、HENDAWI, E.、等。(2022) 采用可再生能源的电力系统暂态不稳定性风险评估。国际电气与计算机工程杂志，12(5)，第 4649-4660 页。https://doi.org/10.11591/ijece.v12i5.pp4649-4660
[20] AGARALA, A., BHAT, S. S., MITRA, A., ZYCHMA, D.，和 SOWA, P. (2022) 与可再生能源集成的多机电力系统的暂态稳定性分析. 能源, 15(13)，4824。
[21] KRISHNAN, V. A. 和 KUMAR, N. S. (2022) 用于可持续增强基于微电网的可再生能源的鲁棒软计算控制算法。混合加拉

鲁法鱼优化-隔离森林方法。可持续计算：信息学与系统，35，100764，https://doi.org/10.1016/j.suscom.2022.100764

[22] KUMAR, R.、DIWANIA, S.、SINGH, R.、ASHFAQ, H.、KHETRAPAL, P. 和 SINGH, S. (2022) 智能混合风电发电场作为静态补偿器以实现整体稳定性以及多机电力系统的控制。ISA 交易，123，第 286-302 页。

[23] LI, C.，等。(2022) 交直流混合电网可再生能源渗透能力评价方法。能源，15(7)，2550。https://doi.org/10.3390/en15072550

[24] AMINE, H. M.、MESSAOUD, H.、OTHMANE, A.、SAAD, M.、ABDALLAH, B. 和 OUSSAMA, H. (2021) 采用光伏和混合储能系统的孤立直流微电网的能源管理策略，评估太阳能条件影响。载于 OUAISSA, M.、OUAISSA, M.、EL HIMER, S. 和 BOULOUARD, Z.（编辑）《通信技术、计算和工程进展》，第 875-887 页。